9. REGIONAL EARTHQUAKES RECORDED BY OCEAN BOTTOM SEISMOMETERS (OBS) AND AN OCEAN SUB-BOTTOM SEISMOMETER (OSS IV) ON LEG 88[1]

Robert K. Cessaro and Frederick K. Duennebier, Hawaii Institute of Geophysics[2]

ABSTRACT

During Deep Sea Drilling Project (DSDP) Leg 88, an ocean sub-bottom seismometer (OSS IV) was placed in Hole 581C, and an array of ocean bottom seismometers (OBS) was deployed about the hole. Together they provided a 75-day continuous recording of seismic activity. The OBS array, recording for 11 days, detected more than 80 regional and teleseismic earthquakes, of which only 10 were located by the National Earthquake Information Service (NEIS). The OSS IV, recording for 64 days, provided records of 660 earthquakes of which 59 were located by NEIS. Low frequency mantle P arrivals are observed as first arrivals for events closer than 12°; high frequency ocean P (P_o) and ocean S (S_o) arrivals are observed for most intermediate to shallow depth events. A traveltime curve based on a sample of 33 earthquakes from 6 to 20° agrees well with previous observations for earthquakes with epicentral distances from 12 to 28° recorded in the ocean. A comparison of the regional, NEIS-located earthquakes recorded on an OBS with those recorded on OSS IV suggests that the borehole seismometer is somewhat more sensitive for earthquake detection than ocean-bottom instruments. This chapter presents a preliminary examination of these excellent data.

INTRODUCTION

During DSDP Leg 88 a seismometer array including five Hawaii Institute of Geophysics (HIG) ocean bottom seismometers (OBS) was deployed about DSDP Hole 581C (Fig. 1), where the HIG ocean sub-bottom seismometer (OSS IV) was subsequently emplaced. The OBS array operated continuously from August 31 to September 11, and OSS IV recorded from September 11 to November 17, 1982. More than 80 regional and teleseismic earthquakes were recorded by the OBS array during its 11-day recording period, and 660 earthquakes were recorded by OSS IV during its 64-day recording period. Data recorded on HIG OBS Y220, which was deployed adjacent to Hole 581C, show that only 10 of the earthquakes recorded during the 11-day period were located by the National Earthquake Information Service (NEIS). Only 59 of the 660 earthquakes recorded by OSS IV during its 64-day period were located by the NEIS. Unfortunately, the OBS recording period overlapped the OSS recording period for only 4 hr. and no earthquakes were recorded by both the OBSs and OSS IV. A group of similar earthquakes occurring along the Kuril Trench region were recorded—some during OBS operation, some during OSS IV operation. These earthquake records permit rough comparisons of earthquake signal-to-noise levels between the two instruments. This report presents results of a first look at these excellent data. Detailed analyses are only beginning.

DATA ACQUISITION

The five HIG OBSs deployed in an array about Hole 581C are isolated sensor package instruments (Byrne et al., 1984) with one vertical 4.5-Hz geophone, one unoriented horizontal 4.5-Hz geophone, and a hydrophone. The seismic signals are recorded continuously on a slow-speed (11 days/tape in this case) analog cassette tape. The OSS IV contains a vertical 4.5-Hz geophone stack and two orthogonal horizontal 4.5-Hz geophone pairs. This system also records continuously on analog tape (65 days). For a complete report on the OSS IV design, see Byrne et al., this volume.

EARTHQUAKE SUMMARY

Historically the northwestern Pacific margin has been a region of extreme seismic activity (Fig. 1). Up to eight events per day were recorded by OBS Y220, but most were not located by NEIS (Fig. 2). The 10 NEIS-located earthquakes recorded on this instrument occurred predominantly in the Kuril Trench region (an active subducting plate margin). Of the 660 earthquakes recorded by OSS IV, 59 were located by NEIS with sources in the Aleutians, Kuriles, Japan, and Izu-Bonin arc regions. The 69 NEIS-located earthquakes are listed in Table 1. Magnitudes (m_b) range from 3.9 to 6.6, and epicentral distances range from 6 to 24°. Earthquakes at greater epicentral distances were recorded and are reported in Butler and Duennebier (this volume). Soviet seismologists have recently provided additional source location data for more than 300 earthquakes which occurred during the recording period. The Japan Meteorological Agency (JMA) earthquake source locations will also provide additional data. Although these data are not included in this preliminary investigation, they will significantly enhance our catalog of located epicenters in future analyses of these data.

HIGH-FREQUENCY P AND S PHASES (P_o AND S_o)

The existence of high-frequency P and S phases associated with oceanic seismic propagation paths has been

[1] Duennebier, F. K., Stephen, R., Gettrust, J. F., et al., *Init. Repts. DSDP*, 88: Washington (U.S. Govt. Printing Office)..
[2] Address: Hawaii Institute of Geophysics, University of Hawaii, 2525 Correa Rd., Honolulu, HI 96822.

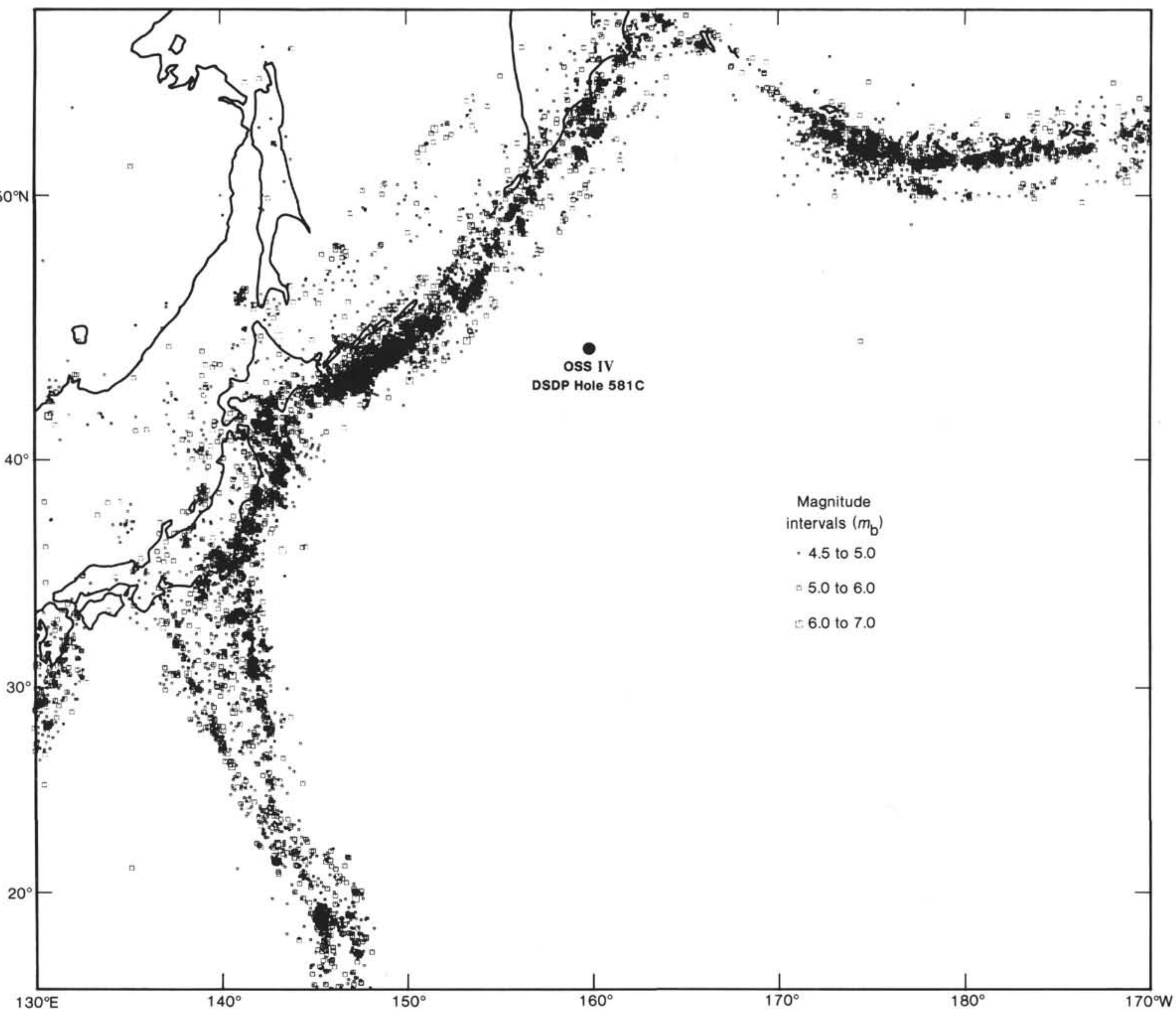

Figure 1. DSDP Hole 581C plotted on an epicentral map of earthquakes located by NEIS from 1912 to 1982 in the region from the Marianas to the Aleutians.

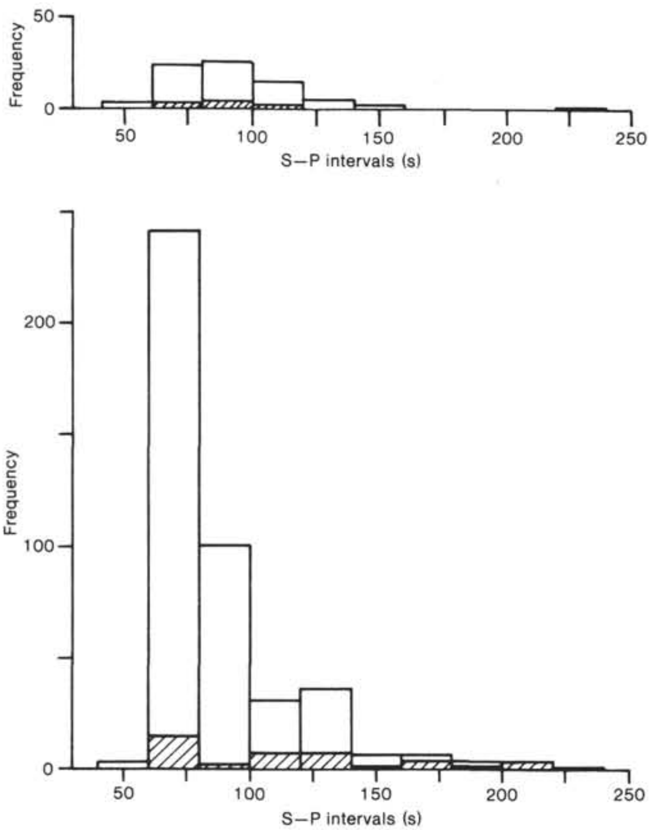

Figure 2. A comparison of the number of earthquakes recorded by HIG's OBS Y220 (above) and OSS IV (below) for different S-P intervals. Hachured areas indicate events located by NEIS.

known for many years. These high-frequency P and S phases have been variously termed but will be called here P_o and S_o (for Ocean P/Ocean S; after Walker, 1984). The P_o/S_o phases are characterized by the predominance of high-frequency energy (dominant frequencies 4–8 Hz), long codas, and efficient propagation over long distances. Recent studies of P_o and S_o phases from earthquakes occurring in the Western Pacific margins have reported on these and other observed characteristics (e.g., Walker and Sutton, 1971; Sutton and Walker, 1972; Asada and Shimamura, 1976; Walker, 1977, 1984; Walker and McCreery, 1983). Energy at 35 Hz has been reported at epicentral distances as great as 18° (2000 km) (Walker and McCreery, 1983). It is the observation of high frequencies at long distances that motivates the general belief that the mode of propagation is by means of some form of a wave guide (e.g., Fuchs and Schulz, 1976; Menke and Richards, 1980; and Gettrust and Frazer, 1981; see Ouchi, 1981 for a useful review of the literature).

P_o traveltimes from a preliminary sample of OSS IV and OBS Y220 earthquake records for event epicentral distances from 6 to 20° (Fig. 3) agree well with the traveltime curve reported by Walker (1977) for epicentral distances from 12 to 28°. Walker (1977) pointed out that the propagation paths for shallow-focus (< 100 km) earthquakes may be approximated by their measured epicentral distance since the P_o wave guide appears to be within the uppermost mantle, possibly near the Mohorovičić discontinuity. Intermediate- to deep-focus (> 100 km)

Table 1. Regional NEIS-located earthquakes recorded on OBS Y220 or OSS IV

No.	Date	Time	Latitude	Longitude	Depth	Mag
1	1982 09 03	03 40 11.8	43.815°N	148.420°E	033	5.8
2	1982 09 03	04 11 57.6	43.774°N	148.471°E	033	5.4
	1982 09 03	07 53 27.9	44.829°N	148.479°E	033	5.1
3	1982 09 03	08 06 41.2	43.724°N	148.479°E	033	5.1
4	1982 09 03	08 28 35.8	43.766°N	148.427°E	033	5.7
5	1982 09 03	10 04 43.7	43.743°N	148.558°E	033	5.0
6	1982 09 06	00 37 59.2	44.020°N	148.283°E	033	4.9
7	1982 09 06	01 47 02.7	29.325°N	140.360°E	176	6.5
	1982 09 06	09 07 37.2	35.619°N	140.683°E	058	4.6
8	1982 09 10	10 20 37.6	55.178°N	161.698°E	033	5.0
9	1982 09 13	18 03 35.8	37.544°N	141.335°E	058	5.1
10	1982 09 14	11 37 22.4	43.476°N	140.153°E	207	5.1
	1982 09 15	10 56 20.7	36.617°N	140.178°E	123	4.4
	1982 09 16	02 20 37.2	30.165°N	139.060°E	368	4.4
	1982 09 16	08 23 12.4	15.707°S	172.745°E	037	5.6
	1982 09 17	13 28 24.8	23.469°S	179.852°W	546	5.9
	1982 09 18	05 46 58.2	31.209°N	140.576°E	066	4.0
	1982 09 18	18 19 37.9	36.200°N	141.384°E	048	4.8
	1982 09 22	10 39 09.3	41.978°N	143.108°E	010	4.8
	1982 09 25	22 06 16.0	37.382°N	135.033°E	374	4.2
11	1982 09 26	01 09 28.5	50.053°N	158.798°E	044	5.5
12	1982 09 26	04 46 37.8	47.015°N	152.289°E	112	5.6
	1982 09 26	08 32 31.5	06.612°N	126.763°E	190	5.4
	1982 09 28	15 14 36.7	24.271°S	176.674°W	040	6.0
13	1982 09 29	09 29 45.6	25.175°N	141.788°E	088	5.0
	1982 09 29	16 10 40.4	25.175°N	140.177°E	081	4.9
14	1982 09 29	20 03 14.7	48.059°N	153.796°E	033	4.4
	1982 10 01	16 53 50.8	37.718°N	139.621°E	145	5.1
15	1982 10 03	23 29 27.9	42.038°N	140.818°E	124	4.7
16	1982 10 04	07 46 52.8	51.435°N	176.620°W	038	5.5
	1982 10 07	11 02 17.3	32.345°N	137.513°E	386	5.1
	1982 10 07	07 15 56.6	07.156°S	125.876°E	515	6.2
17	1982 10 07	21 57 03.6	32.190°N	142.327°E	033	4.8
	1982 10 09	00 53 15.0	40.066°N	143.715°E	033	4.0
	1982 10 13	11 19 12.4	31.980°N	138.251°E	253	3.9
18	1982 10 16	03 02 55.9	34.532°N	139.602°E	121	4.9
19	1982 10 17	18 12 09.0	49.632°N	155.892°E	047	5.5
	1982 10 20	05 36 06.2	40.978°N	143.048°E	040	5.1
20	1982 10 20	11 23 04.0	36.596°N	141.195°E	053	4.7
21	1982 10 20	19 23 10.0	33.613°N	140.949°E	057	4.9
22	1982 10 21	11 10 34.7	52.732°N	172.132°E	033	4.9
23	1982 10 22	02 28 38.0	43.512°N	146.840°E	036	5.0
24	1982 10 23	11 40 57.6	47.340°N	153.360°E	033	4.7
	1982 10 24	15 50 00.3	35.881°N	140.558°E	046	4.7
	1982 10 27	05 45 30.1	46.544°N	152.754°E	033	4.9
	1982 10 27	15 36 36.0	23.951°N	106.049°E	033	5.2
	1982 10 28	03 28 39.1	37.160°N	134.932°E	366	4.8
25	1982 10 28	18 30 30.7	46.307°N	144.100°E	307	4.4
26	1982 10 30	16 25 10.3	51.510°N	157.366°E	033	4.9
	1982 10 30	16 29 59.8	12.194°S	167.463°E	325	5.1
	1982 11 01	08 47 55.1	31.393°N	141.761°E	033	4.4
27	1982 11 04	09 29 53.2	44.045°N	148.040°E	039	5.7
28	1982 11 04	15 54 13.0	38.568°N	143.401°E	033	5.4
	1982 11 07	20 07 39.8	25.866°N	144.490°E	033	4.6
	1982 11 08	16 40 07.5	55.063°N	165.725°E	033	5.2
	1982 11 08	18 35 34.7	04.827°N	127.860°E	160	5.4
	1982 11 09	23 37 16.2	36.575°N	140.620°E	111	5.0
29	1982 11 10	07 36 23.0	44.208°N	149.482°E	033	5.0
	1982 11 10	23 46 32.5	45.210°N	147.924°E	098	4.9
30	1982 11 11	01 55 35.8	44.255°N	149.472°E	033	5.4
31	1982 11 11	02 01 13.4	44.190°N	149.523°E	033	5.0
32	1982 11 11	02 52 08.6	44.181°N	149.481°E	033	5.3
	1982 11 11	04 15 51.5	44.362°N	149.297°E	033	5.0
	1982 11 12	22 08 54.6	43.786°N	149.938°E	033	4.8
	1982 11 13	12 14 04.0	44.872°N	148.750°E	033	4.0
	1982 11 14	08 29 20.3	52.986°N	158.669°E	092	5.7
	1982 11 16	05 12 25.6	39.233°N	144.503°E	033	4.7
	1982 11 16	16 53 32.4	54.341°N	169.055°E	033	4.6
	1982 11 17	09 11 36.5	35.629°N	140.840°E	061	4.6

Note: Recordings of the numbered events are shown in Figure 4; their locations are shown on the map of Figure 5. Mag refers to m_b and depths are in kilometers.

earthquakes, on the other hand, may have propagation paths significantly longer than their epicentral distance and may therefore yield correspondingly lower P_o velocities. P_o arrivals have been examined for 33 earthquakes [numbered events in Table 1 and the Japan May 26, 1982

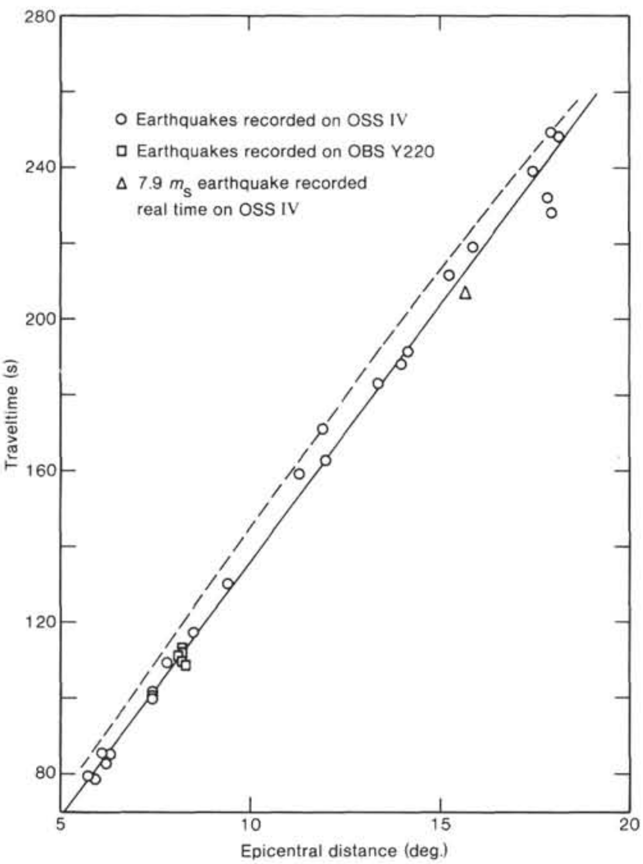

Figure 3. Traveltimes of high frequency P_o phases for events recorded during this study. Traveltime curve for northwestern Pacific P_o phases are shown by the solid line (Walker, 1977). Normal focus mantle refracted P phases for comparison are indicated by the dashed line (Jeffreys and Bullen, 1958).

earthquake (Duennebier, this volume)]. Four events with focal depths greater than 100 km are included in the traveltime graph (Fig. 3). The traveltime versus epicentral distance for the deeper events does not appear to differ significantly from the shallow-focus events. Care must be taken not to confuse the arrival of the low-frequency P, which are refracted in the mantle and seldom contain much energy above 2 Hz, with the P_o at distances less than 12° (cf. Ouchi et al., 1983 and Fig. 4). Accordingly, the low-frequency arrivals were excluded from the traveltime curve presented here. These low-frequency P phases can be seen in Figure 4 for earthquakes numbered 4, 7, 8, 10–12, 23–25, 27–30, and 32. Also, the emergent P_o arrival for Event 13 was not included.

All of the earthquakes recorded by the OBS array (1–8) occurred when there were several ships in the area "making noise." The arrivals marked by the asterisks are identified as explosions from one of the ships. The long coda of the P_o and S_o (top panel) are typical for short period earthquake recordings in the ocean. The P_o coda always decays more slowly than the S_o coda. The energy arriving on the horizontal geophone about 2 s after the P wave arrives at the hydrophone and the vertical geophone is compressional energy converted to shear energy at the sediment/basement interface.

A detailed discussion of each earthquake in Figure 4 follows. The locations of these earthquakes are shown in Figure 5.

The first eight events were recorded by OBS Y220, which was placed adjacent to Hole 581C.

1. Kuril Islands (Sept. 3, 0340Z). The centroid moment solution (NEIS) yields a moment of 8.6 × 10^{24} dyne cm with nodal planes indicating thrust faulting. Typical P_o/S_o arrivals were recorded for this event.

2. Kuril Islands (Sept. 3, 0411Z). This event is actually two events occurring about 40 s apart within 10 km of Event 1. NEIS located only the first of the two. The particle motion for the first of these quakes is quite different from Event 1, possibly indicating different focal mechanisms.

3. Kuril Islands (Sept. 3, 0806Z). This is another aftershock of Event 1, but more similar in waveform and coda to Events 2, 4, and 5.

4. Kuril Islands (Sept. 3, 0828Z). This aftershock was large enough (m_b = 5.7) for a centroid moment solution to be calculated, resulting in a moment of 1.7 × 10^{24} dyne cm, nodal planes and stress axes within 4° of Event 1, and a source location within 10 km. With these similarities, long period arrivals from these two earthquakes must be essentially identical. The OBS records as shown in Figure 4, however, are very different. A closer look at the signals from these earthquakes shows good correlation at frequencies below 1 Hz, but no visible correlation at higher frequencies. This implies that the coda shapes and waveforms of P_o and S_o are not coherent when sources are more than a few km from each other and thus it will be difficult to use P_o and S_o waveforms to determine similarities in source characteristics.

5. Kuril Islands (Sept. 3, 1004Z). Similar to Events 2, 3, and 4.

6. Kuril Islands (Sept. 6, 0037Z). This earthquake occurred about 30 km NE of the preceding events but is still similar in waveform and coda.

7. South of Honshu (Sept. 6, 0147Z). This intermediate depth (176 km) earthquake is notable for its lack of high-frequency energy early in the wavetrain. Many deeper earthquakes (such as Event 10) contain considerably more high-frequency energy early in the record. The coda for Event 7 is somewhat unusual in that the increase to peak amplitudes of the P_o is very slow (>40 s), but still distinctly P_o in character. Whether the lack of high frequencies is a source effect or propagation effect, such as the energy passing through a zone of partial melt, is not known. Most of the path, however, is common oceanic lithosphere. A fault plane solution for this event (NEIS) indicates normal faulting.

8. Near Kamchatka (Sept. 10, 1020Z). The low-frequency precursory arrival for this earthquake indicates that it may be deeper than the 33 km indicated in the NEIS catalog.

The following events were recorded by the borehole seismometer (OSS IV) in the oceanic basement.

9. East coast of Japan (Sept. 13, 1803Z). Because of a large dc offset on the vertical channel, its analog gain was often too low to yield good recordings, as in this example. This low gain, however, allowed the vertical component for larger events (10, 11, 12, 13, etc.) to be recorded without distortion by clipping in the analog tape.

10. Hokkaido (Sept. 14, 1137Z). Although this intermediate depth event (207 km) is rich in high frequencies (compared to Event 7, for example), the P_o and S_o coda are shorter than for most shallow events. Note the obvious low frequency P arrival.

11. Kuril Islands (Sept. 26, 0109Z). Note the obvious low frequency precursor for this event and excellent first motions. The centroid moment solution for this earthquake yields a moment of 1 × 10^{24} dyne cm, an oblique double couple, and east-west compression.

12. Kuril Islands (Sept. 26, 0446Z). This intermediate depth event was located about 500 km west and 200 km south of the previous event. Its centroid moment solution yields a moment of 1.4 × 10^{24} dyne cm and tensional stress perpendicular to the subduction direction.

13. Volcano Island (Sept. 29, 0929Z).

14. Kuril Islands (Sept. 29, 2003Z). Note the well-developed reflection from the ocean surface recorded by the vertical component.

15. Hokkaido, (Oct. 3, 2329Z). Note the very well developed P_o and S_o. The S_o is about four times larger than the P_o (after correcting for the 12 dB gain change).

16. Andreanof Island (Oct. 4, 0746Z). The centroid moment solution yields a moment of 1.6×10^{24} dyne cm, and near north–south compression. The lack of S_0 is typical of earthquakes with significant portions of their paths parallel to the trench axis.

17. South of Honshu (Oct. 7, 2157Z). Note again the poorly developed S_0 arrival.

18. Near South coast of Honshu (Oct. 16, 0302Z). This earthquake is similar to Event 9, showing a well developed S_0 and poorly developed P_0. Note also the early arriving low-frequency energy.

19. Kuril Islands (Oct. 17, 1812Z). The centroid moment solution for this event yields a moment of 1.3×10^{24} dyne cm, and a compressional focal mechanism.

20. Near East coast of Honshu (Oct. 20, 1123Z).

21. South of Honshu (Oct. 20, 1923Z). Similar to Events 9 and 18.

22. Near Aleutian Islands (Oct. 21, 1110Z). This event arriving from the north shows a well developed S_0 arrival.

23. Kuril Islands (Oct. 22, 0228Z)

24. Kuril Islands (Oct. 23, 1140Z)

25. Sea of Okhotsk (Oct. 28, 1830Z). This is the deepest of the displayed regional events (307 km). Note the early low-frequency energy typical of the deeper events.

26. Near Kamchatka (Oct. 30, 1625Z).

27. Kuril Islands (Nov. 4, 0929Z). The centroid moment solution yields a moment of 9.3×10^{23} dyne cm, and a compressional focal mechanism.

28. Off east Honshu (Nov. 4, 1554Z).

29. Kuril Island (Nov. 10, 0736Z).

30. Kuril Island (Nov. 11, 0155Z). This and Event 29 have source locations within a few km of each other and their particle motions are similar but appear inverted in phase.

31. Kuril Island (Nov. 11, 0201Z). This event occurred about 6 min. after and within 10 km of Event 30, yet the coda and frequency content are very dissimilar.

32. Kuril Island (Nov. 11, 0252Z). Note the strong similarities between this and Event 30.

COMPARISON OF OSS IV WITH OBS Y220

A prime motivation for emplacing a seismometer beneath the sediments in solid rock in the ocean bottom was to obtain an improvement in the signal-to-noise ratio for earthquakes. Our experience with OSS II (Carter et al., 1984) suggested that such an emplacement should avoid the noise associated with the sediment/water interface.

A direct comparison between the magnitude threshold (signal-to-noise) of OSS IV and OBS Y220, placed nearby on the ocean floor, cannot be made because no earthquakes were recorded during the short overlap period (4 hr.). The difference in sensitivities can be approximated by determining the range–magnitude threshold for each instrument. A histogram of S–P intervals (Fig. 2) suggests that OSS IV recorded earthquakes for a more complete sample of epicentral distances than OBS Y220. As such, the range–magnitude threshold determined for OBS Y220 may not be as reliable as that for OSS IV. Moreover, as the seismic background noise level may vary with time as much as 18 dB (Duennebier et al., this volume) the threshold of each instrument will also vary. The OSS IV, recording for 64 days, appears to be more sensitive to smaller events at greater distances than those recorded by OBS Y220. An examination of range versus magnitude for OSS IV (Fig. 6) shows many events with magnitudes less than those recorded by OBS Y220. This figure also shows that the events not recorded by OBS Y220 were all at ranges greater than 10° and magnitudes less than 5.5 m_b. OSS IV did not record events below about 5.0 m_b at ranges beyond 30° (Butler and Duennebier, this volume). The picture is far from clear in this preliminary analysis. For certain combinations of ranges and magnitudes, some NEIS-located events were recorded while others were not. However, both the OBS and OSS IV recorded many more earthquakes than were located by the NEIS. When the events located by the Soviet Far East Seismic Network and the Japanese seismic network are included the results should be more meaningful. Future analysis should also reveal what effect variation of background noise has on the threshold of each instrument. There may also be propagation path effects that occult certain earthquake locations for this site (Hart and Kaufman, 1980).

Signal-to-noise as a function of frequency was examined. A subset of two earthquakes, one from OBS Y220 and one from OSS IV, were selected for similar source parameters (depth, magnitudes, focal solutions, and locations). The spectra for these two events are presented in Figure 7. Again, OSS IV seems to be more sensitive in terms of signal-to-noise ratio. For a more complete treatment of signal-to-noise comparisons see Duennebier et al. (this volume).

SUMMARY

An ocean sub-bottom seismometer (OSS IV) and a seismic array including five Hawaii Institute of Geophysics (HIG) ocean bottom seismometers (OBS) were deployed during DSDP Leg 88 approximately 200 km southeast of the Kamchatka Peninsula. The OBS array, recording for 11 days, was followed by a 64-day record made by OSS IV. Of more than 700 regional and teleseismic earthquakes recorded, less than 10% were located by NEIS. This report represents our first look at the data obtained from one OBS adjacent to Site 581 and from OSS IV. Low frequency mantle P arrivals were observed in many earthquakes occurring at epicentral distances less than 12°. High frequency ocean P (P_0) and ocean S (S_0) arrivals were evident for most shallow- to intermediate-depth earthquakes. Traveltimes for a sampling of P_0 arrivals from earthquakes with epicentral distances from 6 to 20° agree with previously reported traveltimes for distances between 12 and 28°. Much work remains to be done on these data. Pooling earthquake source parameters from the Japanese Meteorology Agency and the Soviet Far East seismic networks should permit detailed examination of propagation path characteristics from earthquakes occurring throughout a broad range of distances, azimuths, depths, and tectonic provinces.

ACKNOWLEDGMENTS

This research was funded by the Office of Naval Research. The paper has been reviewed by Dr. Rhett Butler and Dr. Thomas J. Sereno, and edited by Diane Henderson. Hawaii Institute of Geophysics contribution No. 1667.

REFERENCES

Asada, T., and Shimamura, H., 1976. Observation of earthquakes and explosions at the bottom of the Western Pacific: Structure of the oceanic lithosphere revealed by Longshot experiment. *In* Sutton, G. H., Manghnani, M. H., and Moberly, R. (Eds.), *The Geophysics of the Pacific Ocean Basin and Its Margin*: Washington (Am. Geophys. Monogr. Ser.), 19:135–153.

Byrne, D. A., Sutton, G. H., Blackinton, J. G., and Duennebier, F. K., 1984. Isolated sensor ocean bottom seismometer. *Mar. Geophys. Res.*, 5:437–449.

Carter, J. A., Duennebier, F. K., and Hussong, D. M., 1984. A comparison between a downhole seismometer and a seismometer on the ocean floor. *Bull. Seismol. Soc. Amer.*, 74(2):763–772.

Fuchs, K., and Schulz, K., 1976. Tunneling of low-frequency waves through the subcrustal lithosphere. *J. Geophys.*, 42:175–190.

Gettrust, F., and Frazer, L. N., 1981. A computer model study of the propagation of the long-range P_n phases. *Geophys. Res. Lett.*, 8: 749–752.

Hart, R. S., and Kaufman, S. K., 1980. *Seismic Propagation in the Kuriles/Kamchatka region*: Arcadia, California (Sierra Geophysics, Inc.) Technical Report SGI R-80-022.

Jeffreys, H., and Bullen, K., 1958. *Seismological Tables, Office of the British Association:* London (Burlington House).

Menke, H. W., and Richards, P. G., 1980. Crust-mantle whispering gallery phases: a deterministic model of teleseismic P_n wave propagation. *J. Geophys. Res.*, 85(B10):5416–5422.

Ouchi, T., 1981. Spectral structure of high frequency P and S phases observed by OBS's in the Mariana Basin. *J. Phys. Earth*, 29:305–326.

Ouchi, T., Nagumo, S., Kasahara, J., and Koresawa, S., 1983. Separation of high-frequency P_n phases and mantle refracted P phases at distances between 6° and 18° in the Western Pacific by ocean bottom seismograph array. *Geophys. Res. Lett.*, 10(11):1069–1072.

Sutton, G., and Walker, D., 1972. Oceanic mantle phases recorded on seismographs in the Northwestern Pacific at distances between 7° and 40°. *Bull. Seismol. Soc. Amer.*, 62:631–655.

Walker, D. A., 1977. High-frequency P_n and S_n phases recorded in the Western Pacific. *J. Geophys. Res.*, 82(23):3350–3360.

_______, 1984. Deep ocean seismology. *EOS, Trans. Am. Geophys. Union*, 65(1):2–3.

Walker, D. A., and McCreery, C. S., 1983. Spectral characteristics of high-frequency P_n and S_n phases in the Western Pacific. *J. Geophys. Res.*, 88(B5):4289–4298.

Walker, D. A., and Sutton, G. H., 1971. Oceanic mantle phases recorded on hydrophones in the Northwestern Pacific at distances between 9° and 40°. *Bull. Seismol. Soc. Amer.*, 61:65–78.

Date of Initial Receipt: 2 January 1985
Date of Acceptance: 26 March 1985

Figure 4. Selected NEIS-located earthquakes recorded on OBS Y220 (1–8) and OSS IV (9–32). Event location information is given in Table 1. The upper panel shows the vertical component (unless otherwise noted) of particle velocity versus time at a compressed time scale. The absolute particle velocity at high frequencies is represented by a scale to the left of each trace. The other panels show first arrivals for the event on all components at an expanded time scale. Many events were clipped in the recording process, indicated by the letter C above the trace. Gain changes amounting to 6 dB for the OBS and 12 dB for the OSS are indicated by the letter G and an arrow indicating the direction of change. Refraction shots during an earthquake record are indicated by an asterisk (*). High-frequency mantle guided phases are indicated by P_o and S_o, the low-frequency refracted mantle phases are indicated by P. See text for detailed discussions of events.

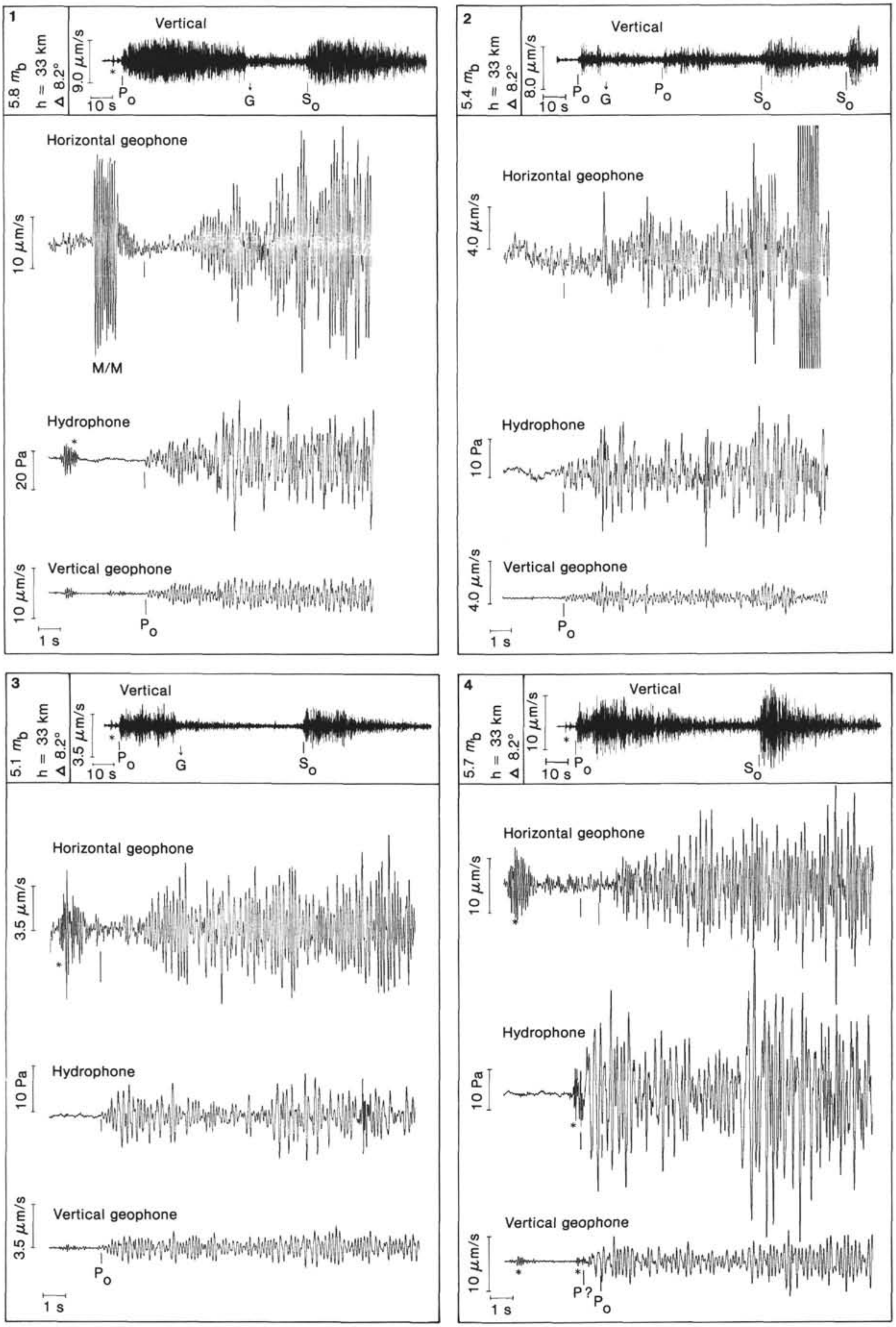
1
5.8 m_b
h = 33 km
Δ 8.2°
Vertical
9.0 μm/s
10 s
P_o
G
S_o
Horizontal geophone
10 μm/s
M/M
Hydrophone
20 Pa
Vertical geophone
10 μm/s
P_o
1 s
2
5.4 m_b
h = 33 km
Δ 8.2°
Vertical
8.0 μm/s
10 s
P_o
G
P_o
S_o
S_o
Horizontal geophone
4.0 μm/s
Hydrophone
10 Pa
Vertical geophone
4.0 μm/s
P_o
1 s
3
5.1 m_b
h = 33 km
Δ 8.2°
Vertical
3.5 μm/s
10 s
P_o
G
S_o
Horizontal geophone
3.5 μm/s
Hydrophone
10 Pa
Vertical geophone
3.5 μm/s
P_o
1 s
4
5.7 m_b
h = 33 km
Δ 8.2°
Vertical
10 μm/s
10 s
P_o
S_o
Horizontal geophone
10 μm/s
Hydrophone
10 Pa
Vertical geophone
10 μm/s
P?
P_o
1 s

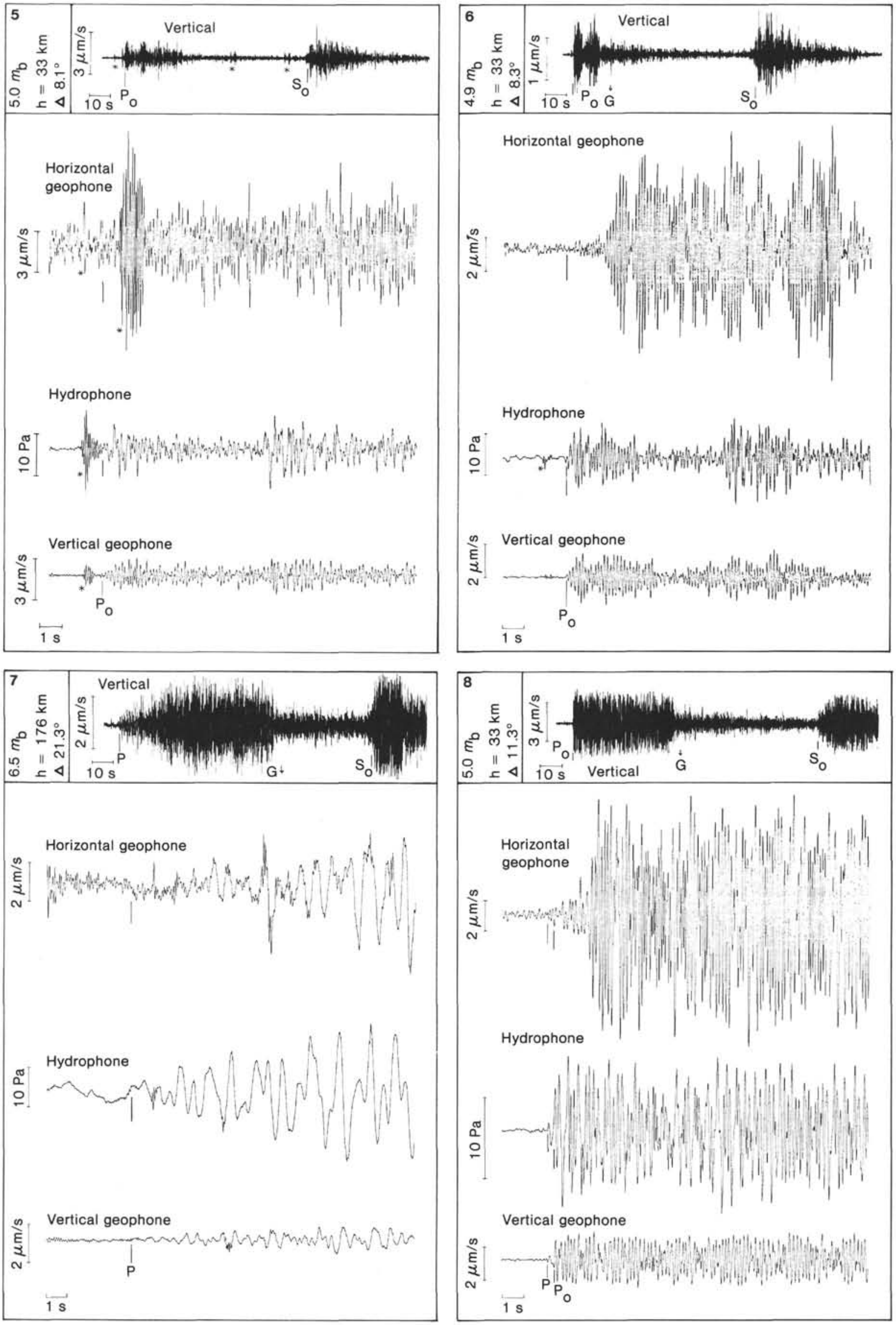

Figure 4 (continued).

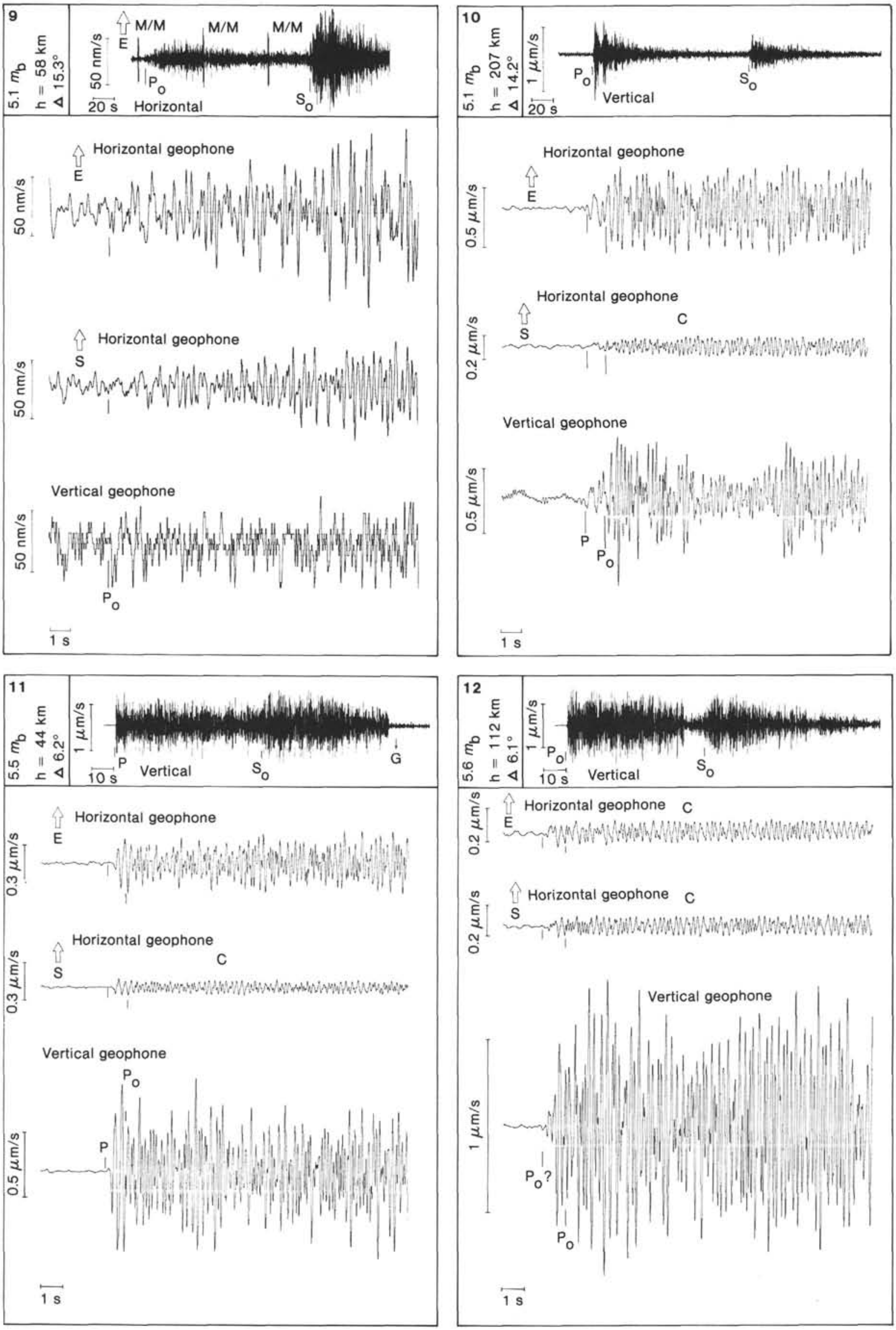

Figure 4 (continued).

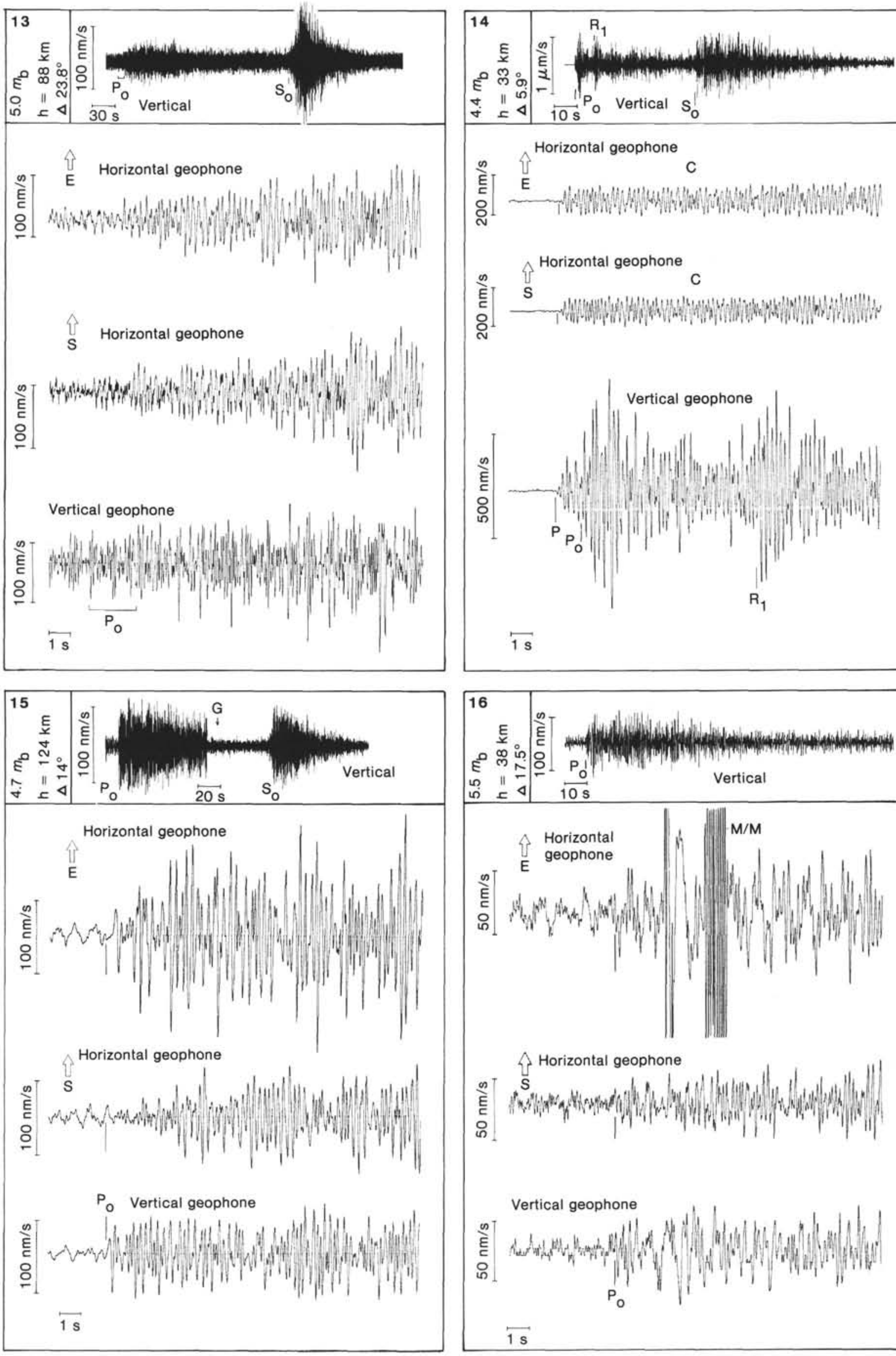

Figure 4 (continued).

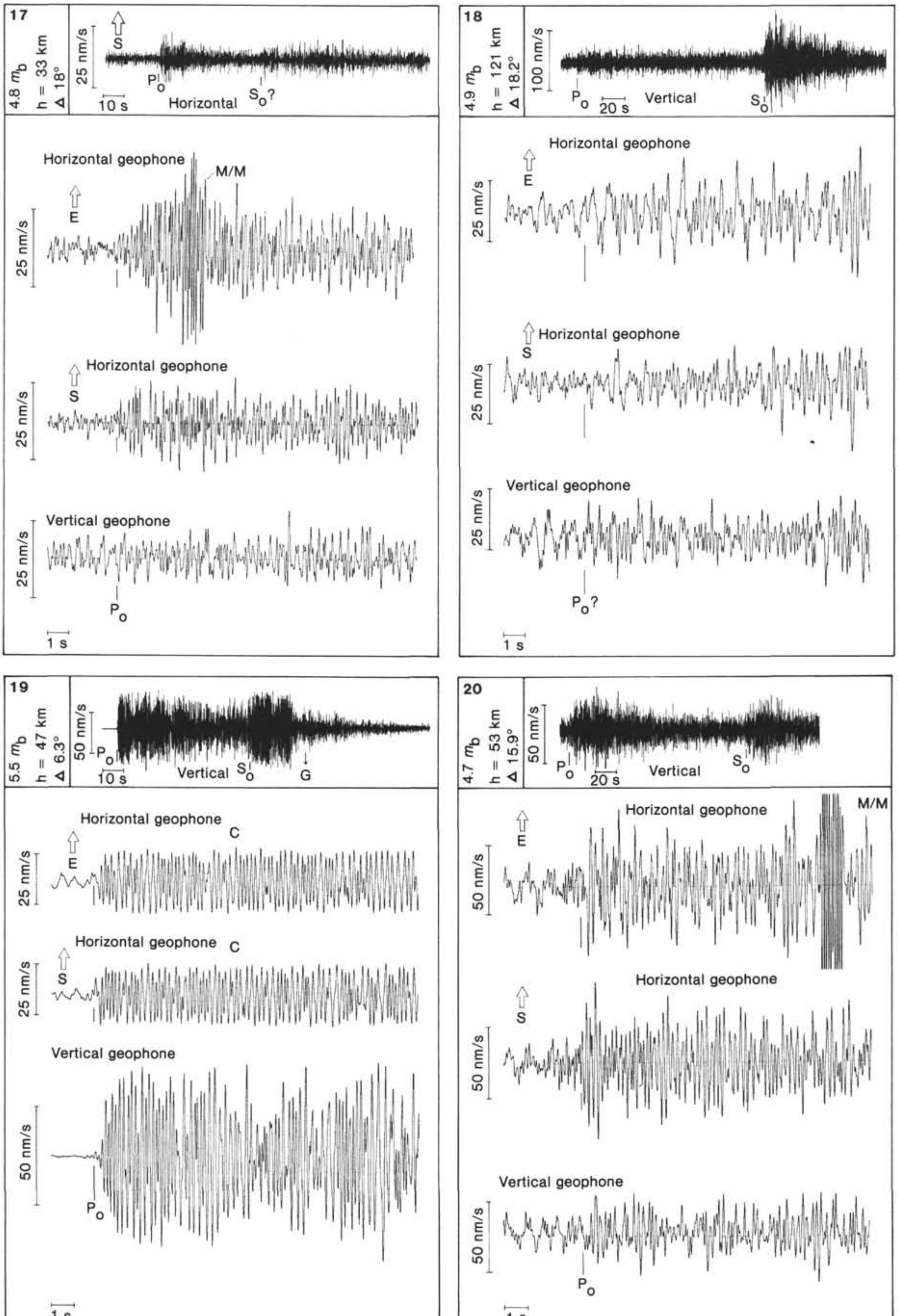

Figure 4 (continued).

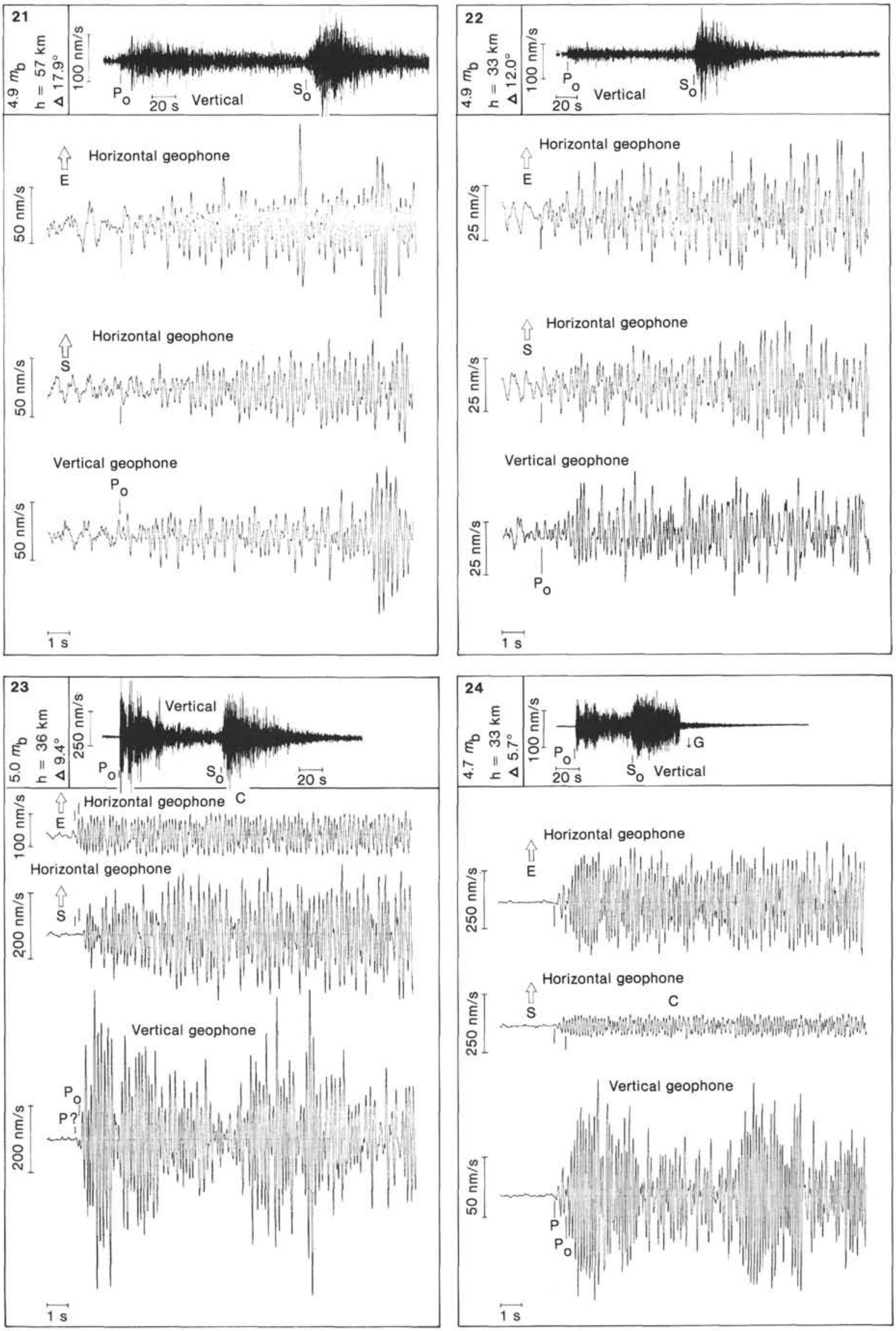

Figure 4 (continued).

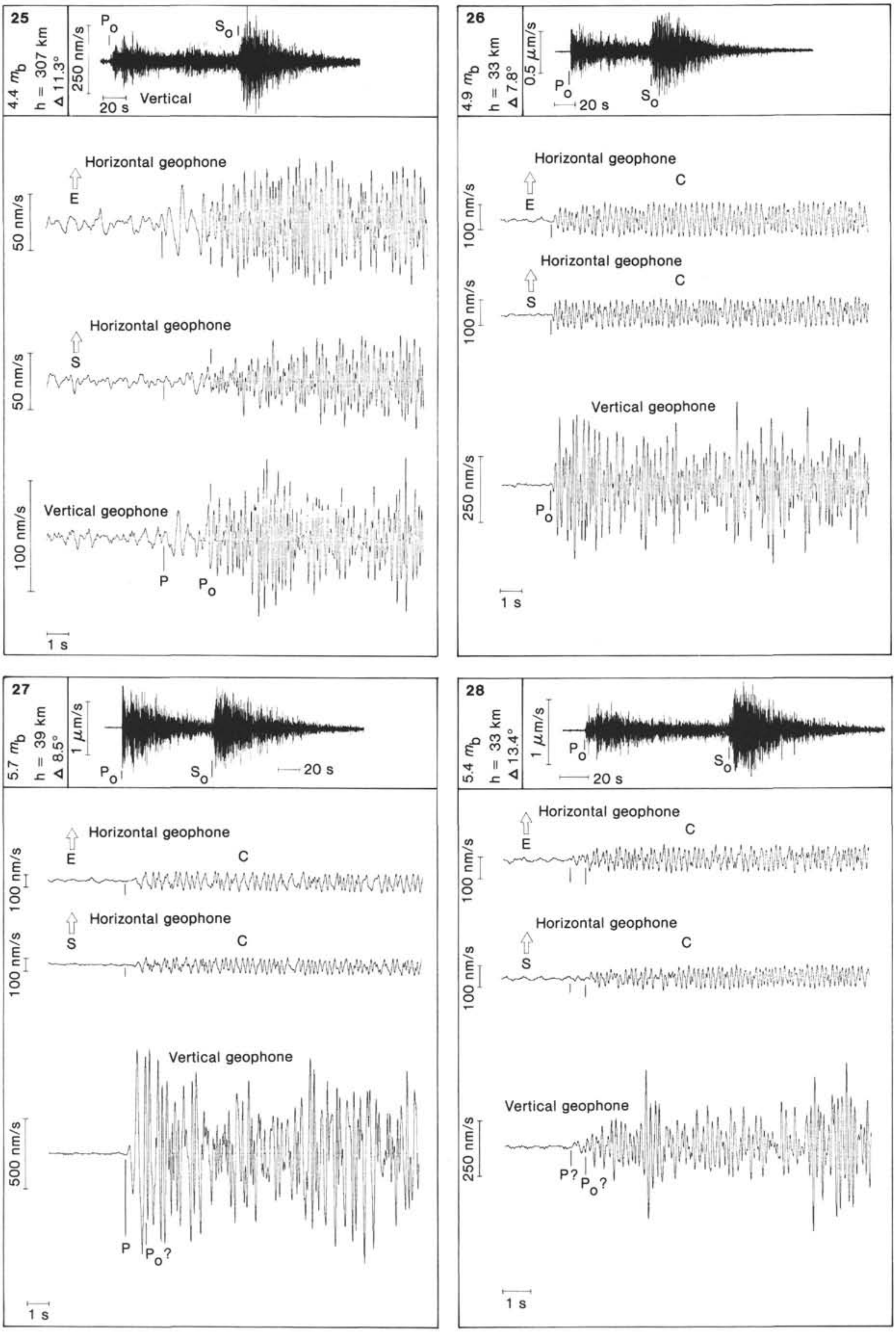

Figure 4 (continued).

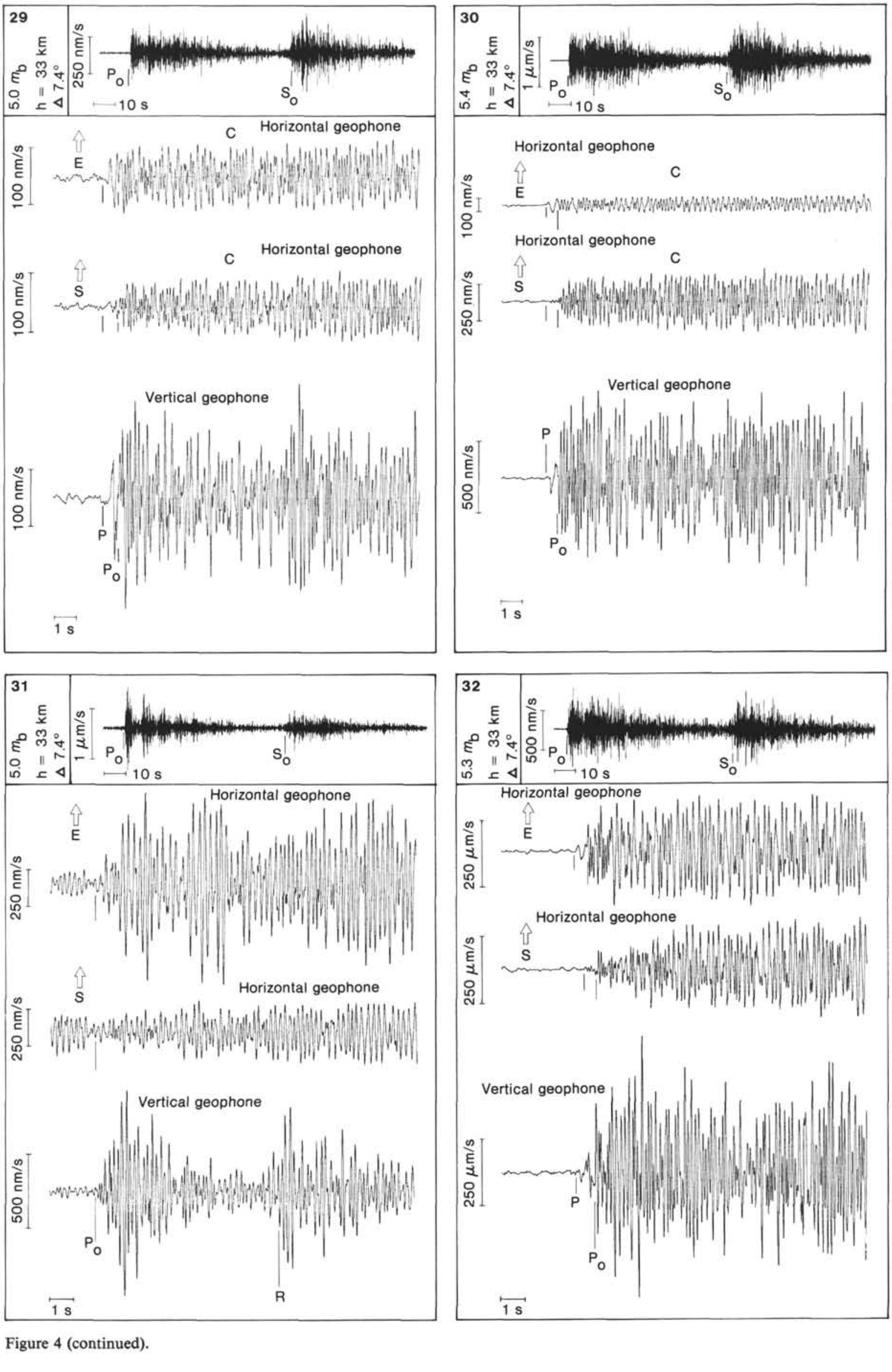

Figure 4 (continued).

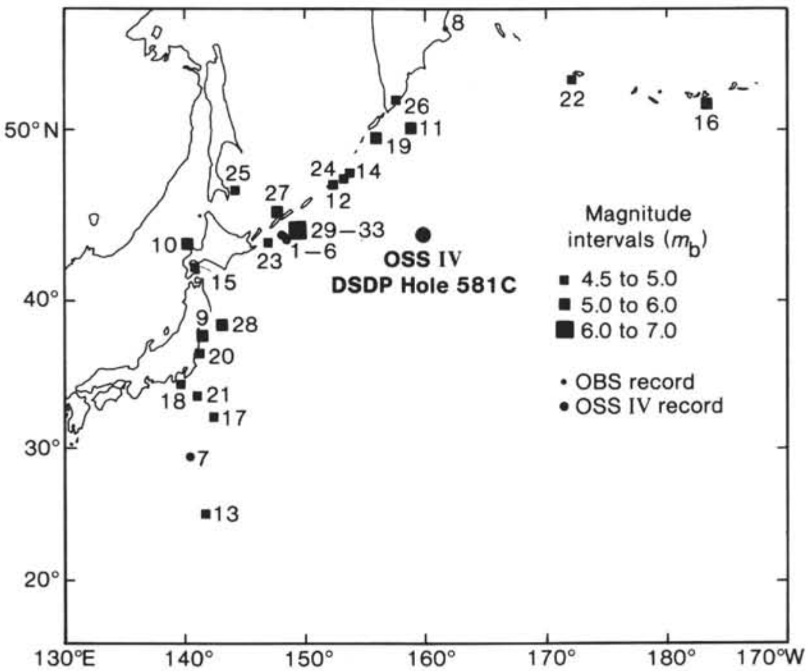

Figure 5. Epicentral map of 33 selected regional earthquakes located by NEIS in the northwestern Pacific and recorded at Hole 581C on OBS Y220 or OSS IV during the DSDP Leg 88 seismic experiment.

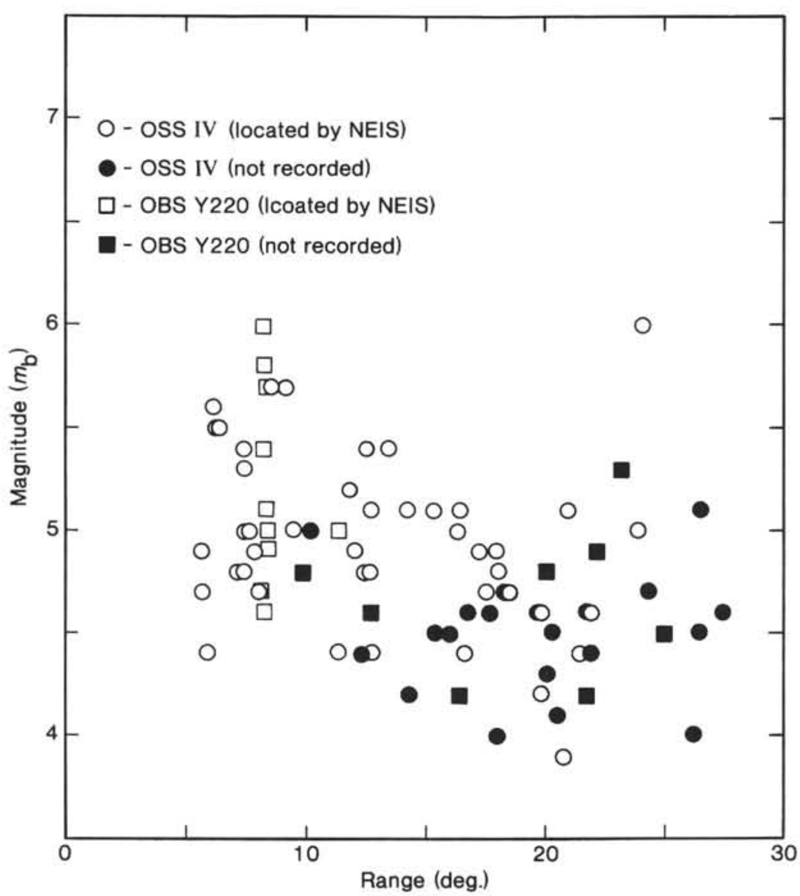

Figure 6. Range versus magnitude for earthquakes located by NEIS and recorded by OBS Y220 and OSS IV. NEIS-located events that were not recorded are denoted by darkened symbols. There is a suggestion of greater sensitivity for OSS IV in view of the number of smaller events recorded.

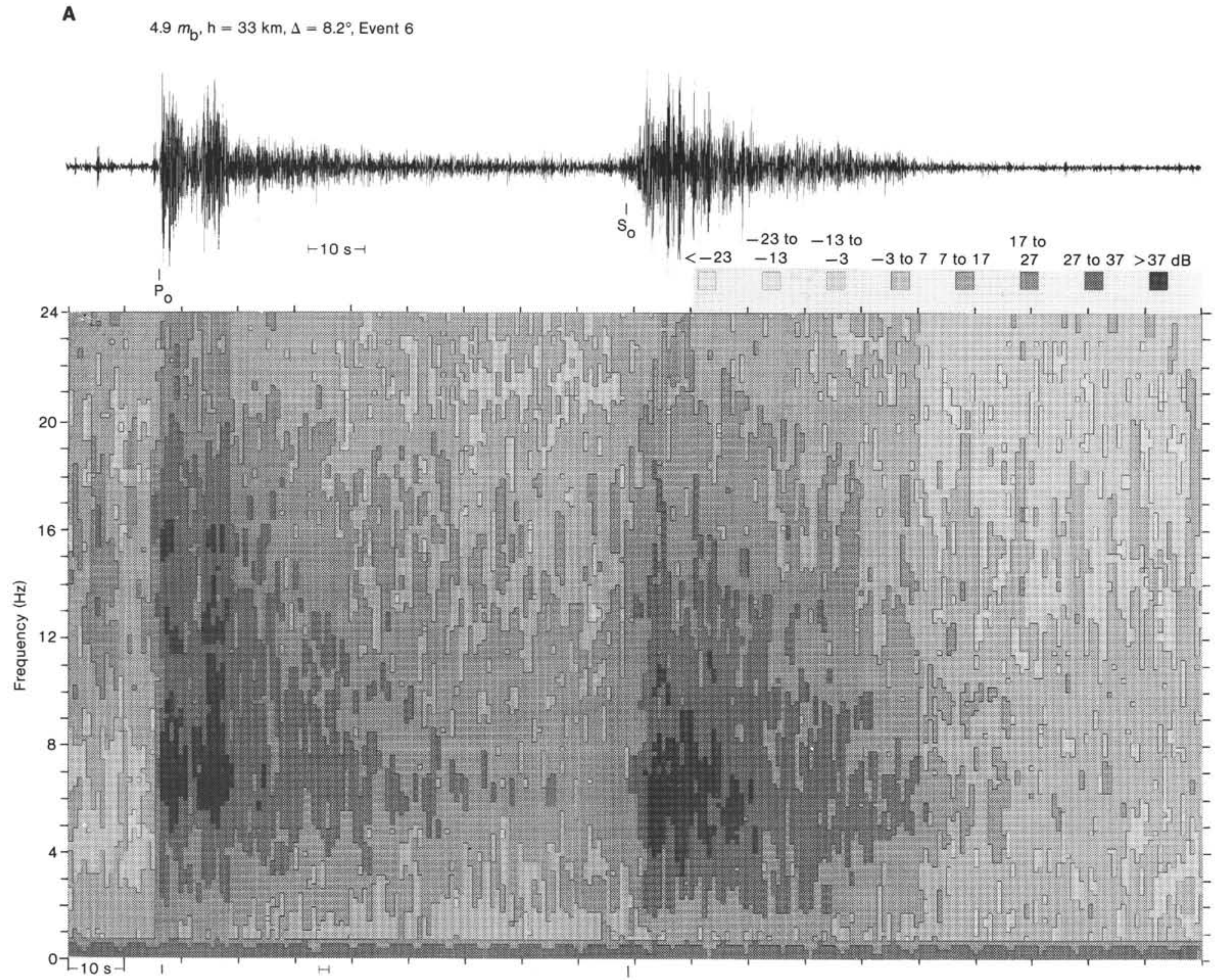
A
4.9 m_b, h = 33 km, Δ = 8.2°, Event 6
10 s
P_o
S_o
< −23
−23 to −13
−13 to −3
−3 to 7
7 to 17
17 to 27
27 to 37
> 37 dB
Frequency (Hz)
0
4
8
12
16
20
24
10 s

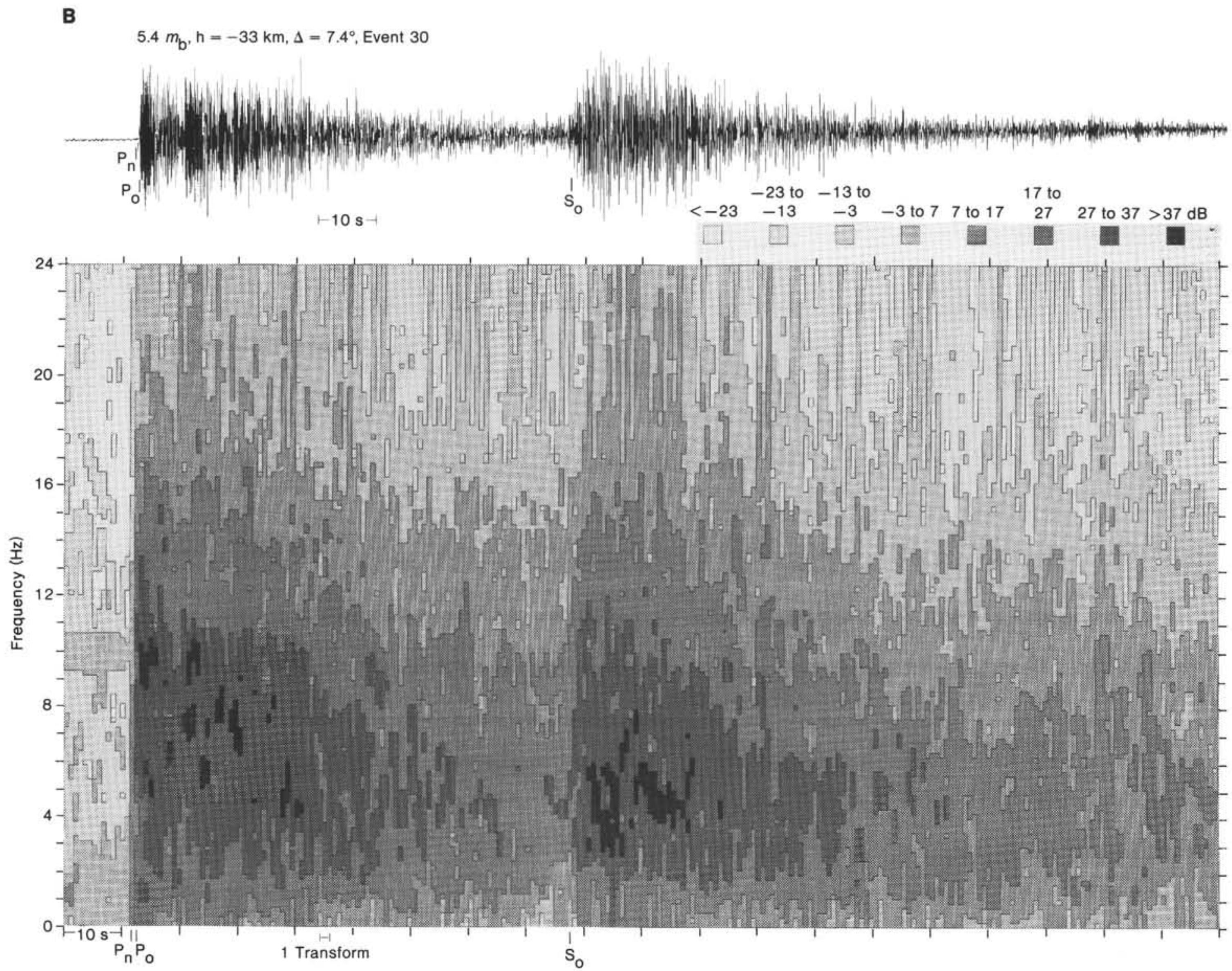

Figure 7. Spectrograms for earthquakes recorded on (A) OBS Y220 and (B) OSS IV. These spectrograms have been made by overlapping 128-point, fast Fourier transforms (FFT) by 50% (40 Hz Nyquist on digitization). The vertical blocks are averages of two adjacent power spectral estimates. The horizontal blocks are from individual 128-point FFTs. The contour interval is 10 dB. The transforms are uncorrected for instrument response or differences in acoustic impedance.